Recursive *T* matrix algorithm for resonant multiple scattering: applications to localized plasmon excitations

Brian Stout,[1,*] J. C. Auger,[2] and Alexis Devilez[1]

[1]*Case 161, Institut Fresnel, Faculté des Sciences et Techniques de St. Jérôme, 13397 Marseille cedex 20, France*
[2]*Center for Laser Diagnostics, Department of Applied Physics, Yale University, New Haven, Connecticut 06520, USA*
[*]*Corresponding author: brian.stout@fresnel.fr*

Received April 24, 2008; revised July 3, 2008; accepted July 4, 2008; posted July 29, 2008 (Doc. ID 95416); published September 22, 2008

A matrix balanced version of the recursive centered *T* matrix algorithm applicable to systems possessing resonant interparticle couplings is presented. Possible domains of application include systems containing interacting localized plasmon resonances, surface resonances, and photonic jet phenomena. This method is of particular interest when considering modifications to complex systems. The numerical accuracy of this technique is demonstrated in a study of particles with strongly interacting localized plasmon resonances. © 2008 Optical Society of America

OCIS codes: 290.4210, 290.5825, 240.5420, 160.4236.

1. INTRODUCTION

It has been well established that certain kinds of recursive *T* matrix algorithms [known as recursive centered *T* matrix algorithms (RCTMAs)] [1,2] are numerically stable and can be used to solve the Foldy–Lax multiple-scattering equations for particles exhibiting "modest" interparticle couplings. By "modest couplings," we refer to situations in which the order of the orbital number of the vector spherical wave functions (VSWFs) necessary to describe the field scattered by each particle in an aggregate of particles is not too much larger than that necessary for describing isolated particles. The modest coupling criteria apply to a host of multiple scattering situations, including systems of dielectric particles comparable in size to the wavelength and for most packing fractions including dense packing. The modest coupling criteria can also apply to metallic particles under certain conditions.

As with any multiple-scattering technique not employing matrix balancing, a user of the RCTMA can encounter numerical difficulties in certain extreme situations of strongly coupled resonant phenomenon. In this work, we present a matrix balanced form of the RCTMA that can readily be employed even in the presence of strong (i.e., resonant) interparticle couplings. The rather extreme situation of "strong couplings" studied here will generally require carefully microscaled, engineered systems where high *Q*-factor resonances can occur for particles illuminated in isolation, and in which the particles are sufficiently closely spaced that neighboring particles modify the resonance response properties. Examples of strong interparticle couplings can be found in particles exhibiting plasmon resonances, surface resonances, or even photonic jet phenomena.

In Section 2, the notation is introduced in a brief review of the relevant multiple-scattering theory. Section 3 describes an analytic matrix balancing procedure used to "well-condition" the multiple scattering system of equations. A matrix balanced RCTMA is derived in Section 4. Essential formulas for applications are summarized in Section 5. Their applications are then demonstrated by applying matrix balanced RCTMA calculations to study systems of interacting localized plasmon excitations. Some known and novel aspects of interacting localized plasmon excitations are presented.

2. MULTIPLE-SCATTERING THEORY: VSWF APPROACH

Let us consider an arbitrary electromagnetic field incident on a collection of three-dimensional particles (as shown in Fig. 1). The particles are considered "individual" scatterers if they can be placed in a circumscribing sphere lying entirely within the homogeneous medium (actually this constraint can frequently be relaxed; see [3]).

The electromagnetic field $\mathbf{E}_i$ incident on an N-particle system is developed in terms of the transverse *regular* VSWFs developed about some point **O** arbitrarily chosen as the system origin:

$$\mathbf{E}_i(\mathbf{r}) = E_0 \sum_{n=1}^{\infty} \sum_{m=-n}^{n} \{\mathrm{Rg}[\mathbf{M}_{nm}(k\mathbf{r})]a_{1,n,m} + \mathrm{Rg}[\mathbf{N}_{nm}(k\mathbf{r})]a_{2,n,m}\}$$
$$= E_0 \sum_{q=1}^{2} \sum_{p=1}^{\infty} \mathrm{Rg}[\mathbf{\Psi}_{q,p}(k\mathbf{r})]a_{q,p} \equiv E_0 \mathrm{Rg}\{\mathbf{\Psi}^t(k\mathbf{r})\}a, \qquad (1)$$

where E_0 is a real parameter determining the incident field amplitude. Equation (1) introduces a condensed notation for the VSWFs $\mathbf{M}_{nm}$ and $\mathbf{N}_{nm}$: $\mathbf{\Psi}_{1,p}(k\mathbf{r}) \equiv \mathbf{M}_{n,m}(k\mathbf{r})$ and $\mathbf{\Psi}_{2,p}(k\mathbf{r}) \equiv \mathbf{N}_{n,m}(k\mathbf{r})$. The notation Rg[ ] stands for "regular part of" and distinguishes these regular VSWFs

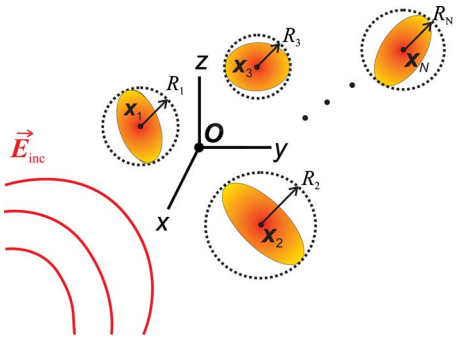

Fig. 1. (Color online) Schematic of a field incident on a collection of scatterers centered on $\mathbf{x}_1, \mathbf{x}_2, \ldots, \mathbf{x}_N$. The radii of the respective circumscribing spheres are denoted $R_1, R_2, \ldots, R_N$.

from "irregular" scattered VSWFs (see Appendix A). In the second line of Eq. (1), the two subscripts n, m are replaced by a single subscript p defined such that $p(n,m) \equiv n(n+1)-m$ and has the inverse relations [4]

$$n(p) = \mathrm{Int}\sqrt{p}, \quad m(p) = -p + n(n+1). \tag{2}$$

The last line of Eq. (1), adopts the compact matrix notation allowing the suppression of the summation symbols [5]. The superscript (^{t}) stands for the transpose of a column "matrix" composed of VSWFs into a row "matrix" of these functions.

For points external to all individual circumscribing spheres, the total field $\mathbf{E}_t(\mathbf{r})$ can be written as the sum of the incident field and a set of individual scattered fields $\mathbf{E}_s^{(j)}$ centered respectively on each of the particle centers:

$$\mathbf{E}_t(\mathbf{r}) = \mathbf{E}_i(\mathbf{r}) + \sum_{j=1}^{N} \mathbf{E}_s^{(j)}(\mathbf{r}_j) = E_0 \mathrm{Rg}[\boldsymbol{\Psi}^t(k\mathbf{r})]a + E_0 \sum_{j=1}^{N} \boldsymbol{\Psi}^t(k\mathbf{r}_j) f_N^{(j)}, \tag{3}$$

where each scattered field $\mathbf{E}_s^{(j)}$ is developed with coefficients $f_N^{(j)}$ on the basis of outgoing VSWFs defined with respect to the associated particle center denoted $\mathbf{x}_j$. The spherical coordinates relative to each scatterer are denoted $\mathbf{r}_j \equiv \mathbf{r} - \mathbf{x}_j$.

The crucial idea of Foldy–Lax multiple-scattering theory is that there exists an excitation field $\mathbf{E}_{\mathrm{exc}}^{(j)}(\mathbf{r})$ associated with each particle that is the superposition of the incident field and the field scattered by all the other particles in the system (excluding the field scattered by the particle itself) [6]. From this definition, the excitation field of the jth particle can be written

$$\mathbf{E}_{\mathrm{exc}}^{(j)}(\mathbf{r}_j) \equiv E_0 \mathrm{Rg}[\boldsymbol{\Psi}^t(k\mathbf{r}_j)] e_N^{(j)} \equiv \mathbf{E}_i(\mathbf{r}) + \sum_{l=1, l\neq j}^{N} \mathbf{E}_s^{(l)}(\mathbf{r}_l) = E_0 \mathrm{Rg}[\boldsymbol{\Psi}^t(k\mathbf{r}_j)] \left[J^{(j,0)} a + \sum_{l=1, l\neq j}^{N} H^{(j,l)} f_N^{(l)} \right], \tag{4}$$

where $e_N^{(j)}$ are the coefficients of the excitation field in a regular VSWF basis centered on the jth particle. In the second line of Eq. (4), we have used the translation–addition theorem [1,4,5] and introduced the notation where $J^{(j,0)} \equiv J(k\mathbf{x}_j)$ is a regular translation matrix and $H^{(j,l)} \equiv H\,[k(\mathbf{x}_j - \mathbf{x}_l)]$ is an irregular translation matrix. Analytical expressions for the matrix elements of $J(k\mathbf{x}_j)$ and $H(k\mathbf{x}_j)$ are given in [1,4].

The other key idea of multiple-scattering theory is that the field $f_N^{(j)}$ scattered by the object is obtained from the excitation field $e_N^{(j)}$ via the 1-body T matrix $T_1^{(j)}$ derived when one considers the particle to be immersed in an infinite homogeneous medium. This relation is then expressed as

$$f_N^{(j)} = T_1^{(j)} e_N^{(j)}. \tag{5}$$

[The index 1 on the $T_1^{(j)}$ indicates that this T matrix concerns an isolated particle, hence its denotation as a 1-body T matrix.] Employing Eq. (5) in Eq. (4), one obtains a Foldy–Lax set of equations for the excitation field coefficients [1,5]:

$$e_N^{(j)} = J^{(j,0)} a + \sum_{l=1, l\neq j}^{N} H^{(j,l)} T_1^{(l)} e_N^{(l)} \qquad j = 1, \ldots, N. \tag{6}$$

For numerical applications where one is obliged to solve the equations on a truncated VSWF basis, it is advantageous to work with a set of formally equivalent equations involving the scattering coefficients $f_N^{(j)}$. This set of equations is derived by multiplying each of Eqs. (6) from the left by $T_1^{(j)}$ and using Eq. (5) to obtain

$$f_N^{(j)} = T_1^{(j)} J^{(j,0)} a + T_1^{(j)} \sum_{l=1, l\neq j}^{N} H^{(j,l)} f_N^{(l)} \qquad j = 1, \ldots, N. \tag{7}$$

In the RCTMA, one calculates the *centered* multiple scattering transition matrices $T_N^{(j,k)}$, which directly yield the scattered field coefficients in terms of the field incident on the system through the expression

$$f_N^{(j)} = \sum_{k=1}^{N} T_N^{(j,k)} a^{(k)} \qquad a^{(k)} \equiv J^{(k,0)} a. \tag{8}$$

In this equation, we have introduced the column matrix $a^{(j)}$ that contains the coefficients of the field incident on the entire system developed on a VSWF basis centered on the jth particle.

3. BASIS SET TRUNCATION AND MATRIX BALANCING

Although the multiple scattering formulas of the previous section are expressed as matrix equations on VSWF basis sets of infinite dimension, the finite size of the scatterers naturally restricts the dimension of the dominant VSWF contributions. To discuss this phenomenon analytically, we consider the case of spherical scatterers. For nonspherical scatterers, the matrix balancing procedure described below should be applied to the circumscribing spheres of the particles.

The Mie solution for a sphere of radius R_j immersed in a homogeneous host medium can be cast in the form of a 1-body T matrix that is diagonal in a VSWF basis centered on the particle:

$$[T_1^{(j)}]_{q,p;q',p'} = \delta_{q,q'}\delta_{p,p'}T_1(j,n(p),q), \tag{9}$$

where the $T_1^{(j)}(n(p),q)$ correspond to the Mie coefficients and depend on q and n [cf. Eq. (1)].

With the objective of matrix balancing, it is helpful to express the Mie coefficients of the scatterers in terms of the Ricatti–Bessel and Hankel functions, respectively, $\psi_n(z) \equiv z j_n(z)$ and $\xi_n(z) \equiv z h_n(z)$, and their logarithmic derivatives

$$\Phi_n(z) \equiv \frac{\psi_n'(z)}{\psi_n(z)}, \quad \Psi_n(z) \equiv \frac{\xi_n'(z)}{\xi_n(z)}. \tag{10}$$

The T matrix elements of Eq. (9) for a sphere of dielectric contrast $\rho_j \equiv k_j/k$ can then be cast in the convenient form [7]

$$\begin{aligned} T(j,n,1) &= \frac{\psi_n(kR_j)}{\xi_n(kR_j)} \frac{(\mu_j/\mu)\Phi_n(kR_j) - \rho_j\Phi_n(\rho_j kR_j)}{\rho_j\Phi_n(\rho_j kR_j) - (\mu_j/\mu)\Psi_n(kR_j)} \\ &\equiv \frac{\psi_n(kR_j)}{\xi_n(kR_j)}\bar{T}(j,n,1), \\ T(j,n,2) &= \frac{\psi_n(kR_j)}{\xi_n(kR_j)} \frac{(\mu_j/\mu)\Phi_n(\rho_j kR_j) - \rho_j\Phi_n(kR_j)}{\rho_j\Psi_n(kR_j) - (\mu_j/\mu)\Phi_n(\rho_j kR_j)} \\ &\equiv \frac{\psi_n(kR_j)}{\xi_n(kR_j)}\bar{T}(j,n,2), \end{aligned} \tag{11}$$

where k is the wavenumber in the external medium. The normalized T matrix coefficients $\bar{T}(j,n,q)$ of Eq. (11) contain a rich resonant structure. The ratios $\psi_n(kR_j)/\xi_n(kR_j)$ on the other hand have an exponentially decreasing behavior for large $n \gg kR_j$ as is demonstrated in Fig. 2 for $kR=10$. One can remark from Fig. 2 that $|\psi_n(kR)/\xi_n(kR)|$ becomes quite small beyond $n_{max}=kR+3$, and its value at $n=14$ is $\sim 2\times 10^{-4}$. Although these factors permit an appropriately truncated VSWF basis set to contain essentially all the physical information necessary for accurate calculations, they also tend to produce ill-conditioned linear systems when one is obliged to enlarge the VSWF space far beyond $\approx kR+3$ to account for strong coupling phenomena.

A solution to the above problem is to balance the matrix manipulations in Section 4 below by defining normalized scattering and incident coefficients

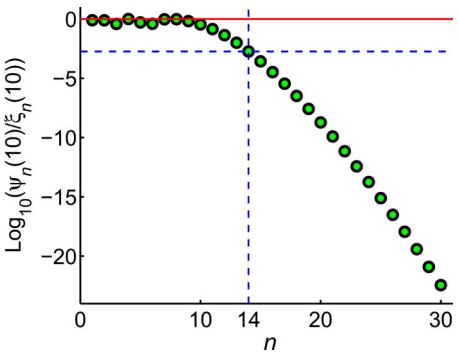

Fig. 2. (Color online) Plot of the spherical Bessel to Hankel function ratio $|\psi_n(kR)/\xi_n(kR)|$ occurring in the Mie coefficients when $kR=10$.

$$\begin{aligned} [\bar{f}^{(j)}]_{q,p} &\equiv \xi_{n(p)}(kR_j)[f^{(j)}]_{q,p}, \\ [\bar{a}^{(j)}]_{q,p} &\equiv \psi_{n(p)}(kR_j)[a^{(j)}]_{q,p}. \end{aligned} \tag{12}$$

For notational purposes, it is convenient to define diagonal matrices $[\psi^{(j)}]$ and $[\xi^{(j)}]$ with Ricatti–Bessel functions along their diagonals, namely, $[\psi^{(j)}]_{q',p';q,p} \equiv \delta_{q,q'}\delta_{p,p'}\psi_{n(p)}(kR_j)$ and $[\xi^{(j)}]_{q',p';q,p} \equiv \delta_{q,q'}\delta_{p,p'}\xi_{n(p)}(kR_j)$. This notation allows normalized or balanced versions of the one-body and many-body T matrices to be defined, respectively, as

$$\bar{T}_1^{(j)} \equiv [\xi^{(j)}]T_1^{(j)}[\psi^{(j)}]^{-1}, \quad \bar{T}_N^{(j,k)} \equiv [\xi^{(j)}]\bar{T}_N^{(j,k)}[\psi^{(k)}]^{-1}. \tag{13}$$

In terms of these normalized quantities, Eq. (8) then reads

$$\bar{f}_N^{(j)} = \sum_{k=1}^{N} \bar{T}_N^{(j,k)}\bar{a}^{(k)} \qquad j = 1, \ldots, N. \tag{14}$$

In the next section, these normalized $\bar{T}_1^{(j)}$ and $\bar{T}_N^{(j,k)}$ are used to derive a matrix balanced version of the recursive T matrix algorithm.

4. DERIVATION OF A MATRIX BALANCED RECURSIVE ALGORITHM

In this section, we derive a matrix balanced version of the RCTMA using purely algebraic manipulations. The recursive algorithm can be invoked once we have a solution for the $\bar{T}_{N-1}^{(j,k)}$ matrices of a $N \geqslant 1$ particle system. If we wish to use only the recursive algorithm to solve a system, we initiate the recursive process with a single particle solution described by $\bar{T}_1^{(1,1)} \equiv \bar{T}_1^{(1)}$.

One then considers an arbitrarily positioned particle being added to the system. The excitation field on a particle N added to the system can be expressed as the superposition of three fields. The first contribution is simply the field incident on the system, the second contribution results from the scattering of the incident field by the $N-1$st cluster of particles onto the particle N, and the third contribution comes from field scattered by the particle N onto the $N-1$st cluster and which returns to the Nth particle as an excitation field. Invoking the translation–addition theorem and Eq. (8), these three contributions can be expressed in matrix form as [1]

$$e_N^{(N)} = a^{(N)} + \sum_{j,k=1}^{N-1} H^{(N,j)}T_{N-1}^{(j,k)}a^{(k)} + \sum_{j,k=1}^{N-1} H^{(N,j)}T_{N-1}^{(j,k)}H^{(k,N)}f_N^{(N)}. \tag{15}$$

Defining now the normalized irregular translation matrices and excitation coefficients, respectively, as

$$\bar{H}^{(j,k)} \equiv [\psi^{(j)}]H^{(j,k)}[\xi^{(k)}]^{-1}, \quad \bar{e}_N^{(j)} \equiv [\psi^{(j)}]e_N^{(j)}, \tag{16}$$

the normalized form of Eq. (15) can be written

$$\bar{e}_N^{(N)} = \bar{a}^{(N)} + \sum_{j,k=1}^{N-1} \bar{H}^{(N,j)}\bar{T}_{N-1}^{(j,k)}\bar{a}^{(k)} + \sum_{j,k=1}^{N-1} \bar{H}^{(N,j)}\bar{T}_{N-1}^{(j,k)}\bar{H}^{(k,N)}\bar{f}_N^{(N)}, \tag{17}$$

where we also used the definitions in Eqs. (12) and (13).

Recalling that the excitation field is linked to the scattered field by the 1-body T matrix via eq. (5), and invoking the definitions of Eqs. (12) and (16) we can write

$$\bar{e}_N^{(j)} = [\bar{T}_1^{(j)}]^{-1}\bar{f}_N^{(j)}. \tag{18}$$

Employing this relation for particle N on the LHS of Eq. (17) and rearranging we obtain

$$\left\{[\bar{T}_1^{(N)}]^{-1} - \sum_{j,k=1}^{N-1} \bar{H}^{(N,j)}\bar{T}_{N-1}^{(j,k)}\bar{H}^{(k,N)}\right\}\bar{f}_N^{(N)} = \bar{a}^{(N)} + \sum_{j,k=1}^{N-1} \bar{H}^{(N,j)}\bar{T}_{N-1}^{(j,k)}\bar{a}^{(k)}. \tag{19}$$

We now take the normalized $\bar{T}_N^{(N,N)}$ matrix to be expressed as

$$\bar{T}_N^{(N,N)} = \left\{[\bar{T}_1^{(N)}]^{-1} - \sum_{j,k=1}^{N-1} \bar{H}^{(N,j)}\bar{T}_{N-1}^{(j,k)}\bar{H}^{(k,N)}\right\}^{-1}. \tag{20}$$

With this assignment, we multiply both sides of Eq. (19) by $\bar{T}_N^{(N,N)}$ and obtain an expression consistent with equation (14):

$$\bar{f}_N^{(N)} = \bar{T}_N^{(N,N)}\bar{a}^{(N)} + \bar{T}_N^{(N,N)}\sum_{j,k=1}^{N-1} \bar{H}^{(N,j)}\bar{T}_{N-1}^{(j,k)}\bar{a}^{(k)} = \bar{T}_N^{(N,N)}\bar{a}^{(N)} + \sum_{k=1}^{N-1} \bar{T}_N^{(N,k)}\bar{a}^{(k)} = \sum_{k=1}^{N} \bar{T}_N^{(N,k)}\bar{a}^{(k)}, \tag{21}$$

where we have assigned the matrix $\bar{T}_N^{(N,k)}$, $k \neq N$ as

$$\bar{T}_N^{(N,k)} = \bar{T}_N^{(N,N)}\sum_{j=1}^{N-1} \bar{H}^{(N,j)}\bar{T}_{N-1}^{(j,k)}. \tag{22}$$

One completes the description of the scattering by the system by remarking that the field scattered by the other particles in the system comprises the superposition of the field that would be scattered by the $N-1$ particle cluster in the absence of the Nth particle, plus the field scattered from the $N-1$ particle cluster originating as a scattered field emanating from the Nth particle. Using again the translation–addition theorem, the field coefficients of $\bar{f}_N^{(j)}$ can in turn be expressed in a form consistent with Eq. (14) as

$$\begin{aligned}\bar{f}_N^{(j)} &= \sum_{k=1}^{N-1} \bar{T}_{N-1}^{(j,k)}\bar{a}^{(k)} + \sum_{k=1}^{N-1} \bar{T}_{N-1}^{(j,k)}\bar{H}^{(k,N)}\bar{f}_N^{(N)} \\ &= \sum_{k=1}^{N-1} \bar{T}_{N-1}^{(j,k)}\bar{a}^{(k)} + \sum_{k=1}^{N-1} \bar{T}_{N-1}^{(j,k)}\bar{H}^{(k,N)}\bar{T}_N^{(N,N)}\bar{a}^{(N)} \\ &\quad + \sum_{l=1}^{N-1}\sum_{k=1}^{N-1} \bar{T}_{N-1}^{(j,l)}\bar{H}^{(l,N)}\bar{T}_N^{(N,k)}\bar{a}^{(k)} \\ &= \bar{T}_N^{(j,N)}\bar{a}^{(N)} + \sum_{k=1}^{N-1} \bar{T}_N^{(j,k)}\bar{a}^{(k)} = \sum_{k=1}^{N} \bar{T}_N^{(j,k)}\bar{a}^{(k)},\end{aligned} \tag{23}$$

where we invoked Eq. (21). In the second and third lines of Eq. (23) we have defined the $\bar{T}_N^{(j,N)}$ and $\bar{T}_N^{(j,l)}$ matrices such that

$$\bar{T}_N^{(j,N)} = \sum_{k=1}^{N-1} \bar{T}_{N-1}^{(j,k)}\bar{H}^{(k,N)}\bar{T}_N^{(N,N)}. \tag{24a}$$

$$\bar{T}_N^{(j,k)} = \bar{T}_{N-1}^{(j,k)} + \sum_{l=1}^{N-1} \bar{T}_{N-1}^{(j,l)}\bar{H}^{(l,N)}\bar{T}_N^{(N,k)}. \tag{24b}$$

At this point, all the $\bar{T}_N^{(j,k)}$ matrices have been obtained and the matrix manipulations in Eqs. (20), (22), and (24) can then be repeated to add as many particles to the system as desired.

Relationship with System Matrix Inversions. Although the recursive algorithm is quite efficient for systems with relatively small numbers of particles, for systems with many particles, one may prefer to try and solve an entire N-particle system directly. A balanced linear system for the entire system corresponding to our recursive algorithm can be obtained by applying the relation of Eq. (5) to the LHS of Eq. (7), then multiplying both sides of the resulting equations by the $[\psi^{(j)}]$ matrix, and finally rearranging to obtain a system of balanced linear equations for the unknown scattering coefficients:

$$[\bar{T}_1^{(j)}]^{-1}\bar{f}_N^{(j)} - \sum_{k=1,k\neq j}^{N} \bar{H}^{(j,k)}\bar{f}_N^{(k)} = \bar{a}^{(j)} \qquad j = 1, \ldots, N, \tag{25}$$

where we used Eqs. (12) and (13). The system of linear equations (25) can in principle be directly solved by inverting the balanced system matrix:

$$\begin{bmatrix} \bar{f}_N^{(1)} \\ \bar{f}_N^{(2)} \\ \vdots \\ \bar{f}_N^{(N)} \end{bmatrix} = \begin{bmatrix} [\bar{T}_1^{(1)}]^{-1} & -\bar{H}^{(1,2)} & \cdots & -\bar{H}^{(1,N)} \\ -\bar{H}^{(2,1)} & [\bar{T}_1^{(2)}]^{-1} & \cdots & -\bar{H}^{(2,N)} \\ \vdots & \vdots & \ddots & \vdots \\ -\bar{H}^{(N,1)} & -\bar{H}^{(N,2)} & \cdots & [\bar{T}_1^{(N)}]^{-1} \end{bmatrix}^{-1} \begin{bmatrix} \bar{a}^{(1)} \\ \bar{a}^{(2)} \\ \vdots \\ \bar{a}^{(N)} \end{bmatrix}. \tag{26}$$

Once we have inverted this system, one can associate each block with a corresponding $\bar{T}_N^{(j,k)}$ matrix as

$$\begin{bmatrix} \bar{f}_N^{(1)} \\ \bar{f}_N^{(2)} \\ \vdots \\ \bar{f}_N^{(N)} \end{bmatrix} = \begin{bmatrix} \bar{T}_N^{(1,1)} & \bar{T}_N^{(1,2)} & \cdots & \bar{T}_N^{(1,N)} \\ \bar{T}_N^{(2,1)} & \bar{T}_N^{(2,2)} & \cdots & \bar{T}_N^{(2,N)} \\ \vdots & \vdots & \ddots & \vdots \\ \bar{T}_N^{(N,1)} & \bar{T}_N^{(N,2)} & \cdots & \bar{T}_N^{(N,N)} \end{bmatrix} \begin{bmatrix} \bar{a}^{(1)} \\ \bar{a}^{(2)} \\ \vdots \\ \bar{a}^{(N)} \end{bmatrix}, \tag{27}$$

which is of the same form as the desired solutions given in Eq. (14).

5. SUMMARY AND APPLICATIONS TO LOCALIZED PLASMON EXCITATIONS

In this section, we will apply the RCTMA to solve systems exhibiting strong interactions between localized plasma resonances. We begin this section by summarizing the balanced recursive algorithm. We then recall some useful formulas for extracting physical quantities from the T matrix. Finally, we carry out some illustrative calculations for strongly interacting systems.

A. Summary of the Balanced RCTMA Algorithm

To implement the RCTMA, one must first solve the 1-body T matrices $T_1^{(1)}, T_1^{(2)}, \ldots, T_1^{(N_{\text{tot}})}$ for all the particles in the system. Normalized versions of the 1-body T matrices and the irregular translation matrices [1,4] $H^{(j,k)}$ are then calculated via

$$\bar{T}_1^{(j)} \equiv [\xi^{(j)}] T_1^{(j)} [\psi^{(j)}]^{-1}, \quad \bar{H}^{(j,k)} \equiv [\psi^{(j)}] H^{(j,k)} [\xi^{(k)}]^{-1}, \quad (28)$$

where the diagonal matrices

$$[\psi^{(j)}]_{q,q',p,p'} = \delta_{q,q'} \delta_{p,p'} \psi_{n(p)}(kR_j)$$

and

$$[\xi^{(j)}]_{q,q',p,p'} = \delta_{q,q'} \delta_{p,p'} \xi_{n(p)}(kR_j),$$

respectively, have Ricatti–Bessel and Ricatti–Hankel functions on the diagonal. (R_j is the radius of the circumscribing sphere of the jth scatterer).

The balanced recursive algorithm is that the solution for the $T_N^{(N,N)}$ matrix is obtained from the T matrices of the $N-1$st system $T_{N-1}^{(j,k)}$ via the matrix inversion in Eq. (20). All the other matrices $\bar{T}_N^{(j,k)}$ with $j \neq N$ or $k \neq N$ are then obtained via matrix multiplications and additions via Eqs. (22) and (24). This process is then repeated as many times as desired.

B. Physical Quantities

When the incident field is a plane wave, it is convenient to express physical quantities in terms of cross sections. Appealing to the far-field approximation of the field, the extinction and scattering cross sections of clusters of N objects can be expressed, respectively, as [8,9]

$$\sigma_{\text{ext}} = -\frac{1}{k^2} \text{Re}\left[\sum_{j=1}^{N} a^{(j),\dagger} f_N^{(j)}\right], \quad \sigma_{\text{scat}} = \frac{1}{k^2} \sum_{j,k=1}^{N} f_N^{(j),\dagger} J^{(j,k)} f_N^{(k)}. \quad (29)$$

It is also possible to produce analytical expressions for local field quantities such as individual absorption cross sections. For lossy scatterers in a lossless host medium, one can obtain individual particle absorption cross sections by integrating the Poynting vector on a circumscribing sphere surrounding the particle to obtain the formula

$$\sigma_{\mathbf{a}}^{(j)} = -\frac{1}{k^2} \text{Re}\{f_N^{(j),\dagger} e_N^{(j)}\} - \frac{1}{k^2} |f_N^{(j)}|^2. \quad (30)$$

In an analogous fashion, optical forces on the particles can be calculated by integrating the Maxwell tensor on a circumscribing sphere surrounding the particle [10,11]. It is frequently convenient to characterize the optical force by vector cross sections $\vec{\sigma}_{\text{opt}}$, defined such that the time-averaged optical force on particles immersed in a liquid dielectric of refraction index n_{med} can be expressed as

$$\mathbf{F}_{\text{opt}} = \|\mathbf{S}_{\text{inc}}\| \frac{n_{\text{med}}}{c} \vec{\sigma}_{\text{opt}}, \quad (31)$$

where $\|\mathbf{S}_{\text{inc}}\| = \|\frac{1}{2}\text{Re}\{\mathbf{E}_{\text{inc}}^* \times \mathbf{H}_{\text{inc}}\}\|$ is the incident irradiance. The binding force and its associated cross section σ_b between two particles separated by a relative position vector $\mathbf{r}_{\text{pos}} \equiv \mathbf{r}_2 - \mathbf{r}_1$ can be defined as

$$F_b \equiv \frac{1}{2}(\mathbf{F}_2 - \mathbf{F}_1) \cdot \hat{\mathbf{r}}_{\text{pos}} \equiv \|\mathbf{S}_{\text{inc}}\| \frac{n_{\text{med}}}{c} \sigma_b. \quad (32)$$

C. Interacting Localized Plasmon Excitations

For those conductors such as the noble metals that support surface plasmon resonances, one can usually observe localized plasmon resonances in sufficiently small particles. These resonances are typically dominated by absorption if the particles are sufficiently small with respect to the incident wavelength and by scattering for larger particles. We choose to study silver spheres 50 nm in diameter immersed in air (for which both scattering and absorption are nonnegligible).

The study is carried out for wavelengths ranging from the near ultraviolet through the visible (300 to 850 nm). We ignore the relatively modest finite size corrections to damping [12], simply adopt the bulk dielectric constant of silver from [13], and extrapolate between the experimental values. The extinction, scattering, and absorption cross sections for these particles are readily obtained from Mie theory and are displayed in Fig. 3 as a function of frequency. These spheres are quite small with respect to visible wavelengths (size parameters in the 300–800 nm wavelength range go through $kR = 0.52-0.20$), and the isolated particle cross sections are obtained to high precision with $n_{\max} = 4$. One can also see from Fig. 3 that the strength of the plasmon resonance for these particles is about half due to absorption and about half due to scattering.

One of the principle sources of interest in localized plasmon resonances is their capacity to produce large field enhancements in regions much smaller than the incident field wavelength. This property is demonstrated in Fig. 4(a) with a 2D and 1D plot of the electric field intensity in and near an isolated 50 nm diameter silver sphere illuminated near its resonance peak ($\lambda_0 = 365$ nm with $N_{\text{Ag}} = 0.077 + 1.6i$). The plots in Fig. 4 are performed in a plane containing the center of the sphere and perpendicular to $\mathbf{k}_{\text{inc}}$ (the polarization lies along the horizontal axis). The dimensionless extinction and scattering efficiencies $Q = \sigma/(\pi R^2)$ at this frequency are respectively, $Q_{\text{ext}} = 14.48$ and $Q_{\text{scat}} = 6.76$.

We now use the balanced recursive technique to calculate the optical response of a dimer composed of 50 nm diameter silver spheres whose surfaces are separated by

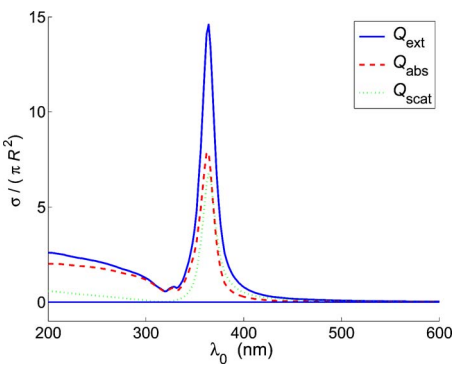

Fig. 3. (Color online) Total cross section efficiencies $Q \equiv \sigma/(\pi R^2)$ for an isolated 50 nm diameter sphere.

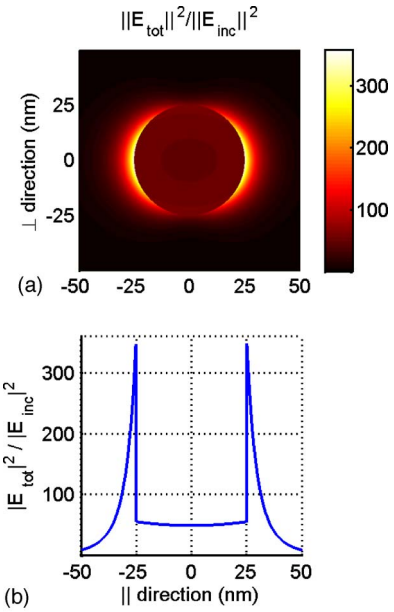

Fig. 4. (Color online) Electric field intensity $\|\mathbf{E}_t\|^2/\|\mathbf{E}_{\text{inc}}\|^2$ in an isolated 50 nm diameter sphere ($\lambda_0=365$ nm, $N_{\text{Ag}}=0.077+1.6i$). (a) 2D (hot) plot of the electric field intensity in a plane perpendicular to the wave vector and containing the origin (horizontal axis lies along the polarization direction). (b) 1D plot of the field intensity along the line in this plane containing the direction of electric field polarization.

1 nm. Although the T matrix calculated by RCTMA contains information for arbitrary incident fields, we study the physically interesting case of a plane wave perpendicular to the axis separating the particles. As is widely known, the response then depends strongly on the polarization of the incident light. In Figs. 5(a) and 5(c), the extinction and scattering cross sections per particle are presented when the polarization is, respectively, perpendicular and parallel to the symmetry axis. From Fig. 5(c), one sees that the cross section for the parallel-to-axis polarization presents a two-sphere coupled resonance that is strongly redshifted with respect to the isolated particle resonance. The polarization perpendicular

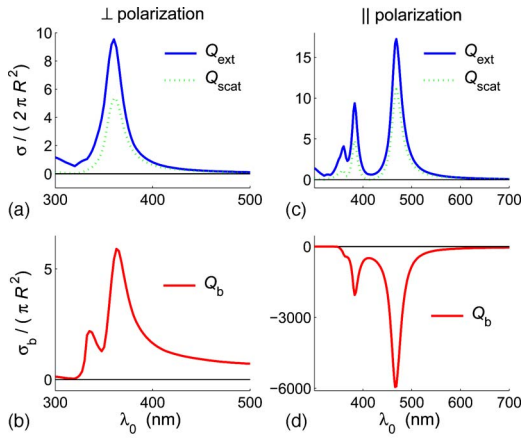

Fig. 5. (Color online) Dimensionless cross section efficiencies per particle $Q=\sigma/(2\pi R^2)$ and binding force efficiencies for a dimer of 50 nm diameter spheres (1 nm separation). In (a) and (b) the polarization is perpendicular to the symmetry axis, and in (c) and (d) it is parallel to the symmetry axis.

to this axis, on the other hand, presents only slight modifications with respect to an isolated sphere.

The optical binding force cross sections for these same polarizations are plotted, respectively, in Figs. 5(b) and 5(d). While the binding force for the polarization perpendicular to the particle axis [see Fig. 5(b)] is slightly repulsive, the force for polarization parallel to the resonance can be highly attractive with the dimensionless $|Q_b|$ attaining amplitudes of three orders of magnitude. There has already been experimental and theoretical evidence supporting the existence of optical force couplings in particles with plasmon excitations [14], although such high-precision calculations at such small separations seems not to have been presented before now.

This dimer system dramatically illustrates the strong coupling category since correct calculations require that the VSWF space be enlarged far beyond the predominantly dipolar response characterizing the particles in isolation. The normalized cross sections per particle are given in Table 1 for different values of the VSWF space truncation. Although it was necessary to go to $n_{\max}\simeq 30$ to achieve four-digit precision in all the cross sections, the table indicates that results were already quite good at $n_{\max}=20$.

A base 10 logarithmic intensity field map for a two-silver-sphere dimer illuminated with light polarized along the symmetry axis [frequency near the coupled sphere resonance maximum ($\lambda_0=467$ nm and $N_{\text{Ag}}=0.048+2.827i$)] is presented in Figs. 6(a) and 6(b), which are, respectively, a 2D plot (in the same plane as Fig. 4) and a 1D plot along the symmetry axis. The size parameter of the individual spheres is $kR=0.34$ and the isolated cross sections at this frequency are $Q_{\text{ext}}=0.136$ and $Q_{\text{scat}}=0.0963$. As can be seen in Fig. 6, the fact that one had to go so far beyond the dipolar response has a dramatic effect on the field inside and near the particles. Notably, the fields inside the particles are no longer quasi-constant as was the case for isolated particles.

An important word of caution should be made at this point. Although 1 nm separation may appear to be nearly touching, the coupled resonance is in fact quite sensitive to exact separation details when resonant particles are so closely separated. For example, at a separation of 0.5 nm for the silver dimer, the coupled plasmon resonance is displaced to $\lambda_0\simeq 516$ nm as compared with $\lambda_0\simeq 467$ nm for a 1 nm separation, and the multipole order has to be pushed to $n_{\max}\simeq 50$ to achieve four-digit accuracy in the cross sections.

Nanometer scale separations are not necessarily theoretical idealizations, however, as recent experiments with DNA separators have demonstrated [15]. Nevertheless, in applications like DNA separators, one may well have to consider the strong optical forces between these particles on account of the exceptionally strong attractive optical force efficiencies of these resonances. For instance, the binding force efficiency at 0.5 nm separation was calculated at $Q_b=-20174$ for $\lambda_0\simeq 515.6$ nm (cf. $Q_b=-6018$ for 1 nm separation at $\lambda_0\simeq 467$ nm). The question of perfect spheres exactly in contact, however, seems untenable from an experimental standpoint and quite difficult from a theoretical standpoint on account of the singular behavior of the contact point. Theoretical separations of 0.1 nm,

Table 1. Dimensionless Cross Section Efficiencies per Particle as a Function of VSWF Truncation n_{max}

n_{max}	5	10	15	20	25	30	35	40
$Q_{ext}/2^a$	4.60	15.53	17.38	17.20	17.14	17.13	17.13	17.13
$Q_{scat}/2$	3.51	10.62	11.30	11.04	10.98	10.97	10.97	10.97
Q_b	−417	−3639	−5530	−5918	−6000	−6015	−6018	−6018

[a] $Q_{ext}=\sigma_{ext}/(2\pi R^2)$, $Q_{scat}=\sigma_{scat}/(2\pi R^2)$, $Q_b=\sigma_b/(\pi R^2)$. The system is a dimer composed of 50 nm diameter silver spheres (1 nm separation) at $\lambda_0=467$ nm and $N_{Ag}=0.048+2.827i$.

for instance, require multipole truncations of the order of $n_{max}\gtrsim 120$ before convergence is achieved, but the idea of "perfect" spheres separated at atomic scales has clearly gone beyond the domain of applicability of our mesoscopic physical model in any case.

It is also important to verify that the recursive algorithm works for more complicated systems. To this end, we illustrate in Fig. 7 the results of calculations for a system composed of a line of five identical silver spheres, each separated by 1 nm. For the binding force, we now present $Q_{b,1}$ as the binding optical force between the two outermost spheres and their nearest neighbors and $Q_{b,2}$ as the binding force between the central sphere and each of its nearest neighbors. It is interesting to remark that the addition of other spheres in the chain dramatically lessens the strong binding force interactions between spheres, even though the fields between the spheres (see Fig. 5) can still be almost as high as in the dimer case.

We remark that the interactions have continued to redshift and widen the coupled "chain" resonance. This chain resonance peaks at ≈ 561 nm and $N_{Ag}\simeq 0.0564+3.685i$ ($Q_{ext}/5=14.416$ and $Q_{scat}/5=12.543$). It is clear from Fig. 7(c) that the extinction cross section of the chain resonance is increasingly dominated by scattering rather than absorption. The number of VSWF orders necessary for high precision was also seen to decrease slightly for the chain. The calculation of Fig. 7 was carried out at $n_{max}=20$ since calculations at $n_{max}=24$ produced negligible differences on this scale.

Despite the dominance of scattering, a considerable amount of absorption is still present in the five-sphere chain. Furthermore, from the field maps in Figs. 6(c) and 6(d), one can see that the central sphere has the highest internal field intensities, and one consequently expects increased absorption in the central sphere. This supposition can readily be confirmed quantitatively by using Eq. (30) to calculate the absorption in each individual sphere. The results are given in Table 2.

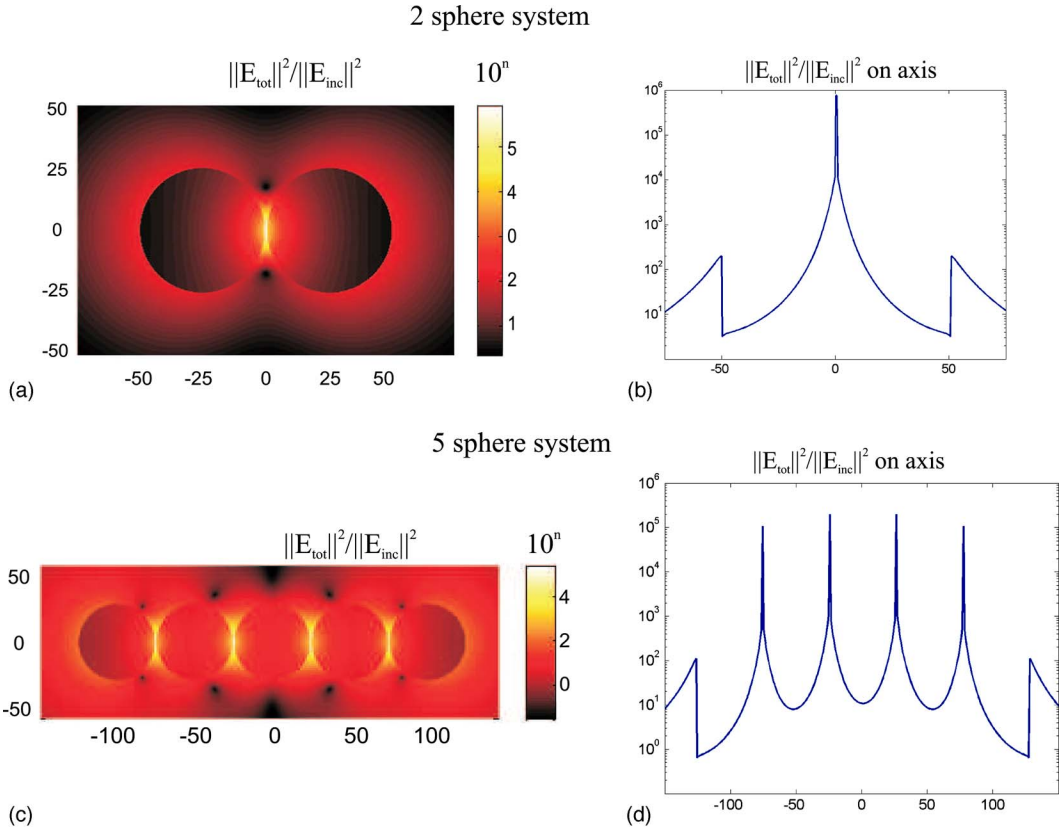

Fig. 6. (Color online) Logarithmic scale plots of the field intensity for a two-sphere dimer with $\lambda_0=467$ nm, $N_{Ag}=0.048+2.827i$, and incident light polarized along the sphere axis. (a) 2D plot in the plane containing the centers of the spheres and the polarization vector. (b) 1D logarithmic plot along the symmetry axis of the spheres. (c) and (d) are the same as (a) and (b), respectively, but for a five-sphere chain of spheres at its resonance maximum ($\lambda_0=561$ nm, $N_{Ag}=0.0564+3.685i$). (cf. Fig. 7).

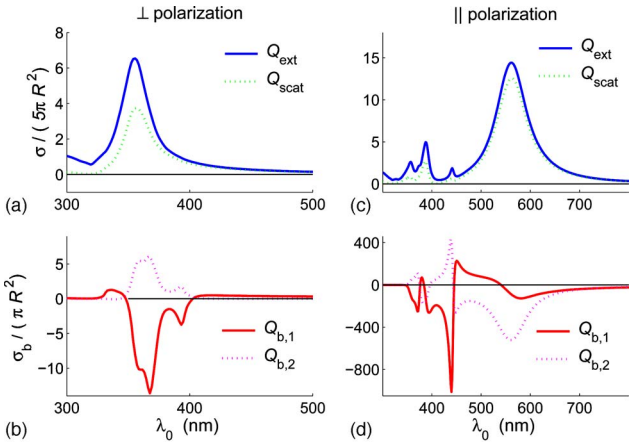

Fig. 7. (Color online) Total cross section and binding efficiencies for a chain of five "touching" silver spheres 50 nm in diameter (1 nm separation). In (a) and (b) the polarization is perpendicular to the symmetry axis, (c) and (d), parallel to the symmetry axis.

Table 2. Individual Absorption Efficiencies $Q_{a,j} \equiv \sigma_{a,j}/(\pi R^2)$ in a Five-Sphere Chain[a]

$Q_{a,1}$	$Q_{a,2}$	$Q_{a,3}$	$Q_{a,4}$	$Q_{a,5}$
0.8346	2.333	3.030	2.333	0.8346

[a]At $\lambda_0 = 561$ nm and $N_{Ag} = 0.0564 + 3.685i$.

We conclude this section with some calculations concerning larger chains of particles. One can remark that the chain coupled resonance continued to redshift and widen when passing from the dimer to the five-particle chain. Results for the extinction and scattering cross sections for chains of 10 and 20 spheres are presented in Fig. 8 for the same polarizations and incident directions as considered previously.

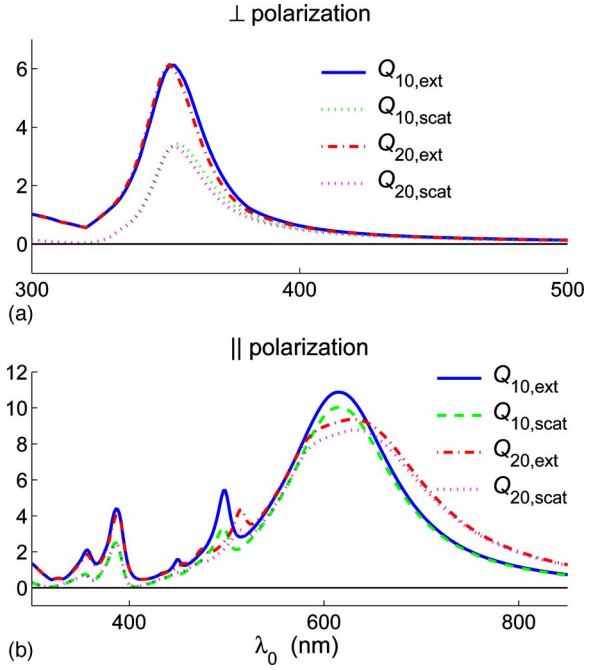

Fig. 8. (Color online) Total extinction and scattering cross section efficiencies per particle in chains of 10 and 20 particles. In (a) the polarization is perpendicular to the symmetry axis, (b), parallel to the symmetry axis.

One readily sees that ultraviolet and perpendicular polarization responses per particle seem to have stabilized for large chains. The collective chain response on the other hand continues to broaden and slightly redshift as one passes from 10- to 20-sphere chains. It is an interesting point for future studies to examine the evolution of this phenomenon for even longer chains and to study the impact of defaults in the chains.

6. CONCLUSIONS

The balanced recursive algorithm can give useful and highly accurate information in systems with large numbers of strongly interacting resonances. This has been demonstrated herein for the case of localized plasmon resonances, and the studies presented here suggest that chains of closely spaced localized plasmons can have potentially interesting applications with respect to frequency shifting and broadening. Although not demonstrated here, this technique also proves useful for treating closely spaced systems possessing surface resonances of whispering gallery type.

It is worth remarking that matrix balancing seems to be a useful method to employ in almost any Foldy–Lax equation solution scheme, be it for direct system matrix inversion, iterative techniques, or linear system solutions. In fact, some modern matrix inversion programs actually integrate numerical matrix balancing into their algorithms. Nevertheless, since the matrix balancing in Foldy–Lax equations can be obtained analytically at relatively low computational cost, it seems beneficial to carry out this balancing explicitly rather than relying on purely numerical treatments.

The matrix balanced RCTMA has potentially interesting applications for other kinds of resonance phenomenon, notably whispering gallery modes. Such studies are currently underway. Furthermore, the ability of the matrix balanced RCTMA to study defaults and small modifications in large complicated systems is particularly promising and will be employed in subsequent studies.

APPENDIX A: VECTOR SPHERICAL WAVE FUNCTIONS

The vector spherical wave functions can be readily written in terms of the vector spherical harmonics (VSHs) and outgoing spherical Hankel functions:

$$\boldsymbol{\Psi}_{1,p}(k\mathbf{r}) \equiv \mathbf{M}_{nm}(k\mathbf{r}) \equiv h_n^+(kr)\mathbf{X}_{nm}(\theta,\phi),$$

$$\boldsymbol{\Psi}_{2,p}(k\mathbf{r}) \equiv \mathbf{N}_{nm}(k\mathbf{r}) \equiv \frac{1}{kr}[\sqrt{n(n+1)}h_n^+(kr)\mathbf{Y}_{nm}(\theta,\phi) + [krh_n^+(kr)]'\mathbf{Z}_{nm}(\theta,\phi)]. \quad \text{(A1)}$$

In the same manner, the regular VSWFs are obtained by replacing the spherical Hankel functions in Eq. (A1) by spherical Bessel functions. Our adopted definition of the VSHs is

$$\mathbf{Y}_{nm}(\theta,\phi) \equiv \hat{\mathbf{r}} Y_{nm}(\theta,\phi), \quad \mathbf{Z}_{nm}(\theta,\phi) \equiv \frac{r\,\boldsymbol{\nabla} Y_{nm}(\theta,\phi)}{\sqrt{n(n+1)}},$$

$$\mathbf{X}_{nm}(\theta,\phi) \equiv \mathbf{Z}_{nm}(\theta,\phi) \wedge \hat{\mathbf{r}}, \tag{A2}$$

where the $Y_{nm}(\theta,\phi)$ are the scalar spherical harmonics.

ACKNOWLEDGMENTS

Brian Stout and Alexis Devilez thank Ross McPhedran, Evgeny Popov, and Nicolas Bonod for helpful discussions. This work was funded in part by the grant ANR-07-PNANO-006-03 ANTARES of the French National Research Agency.

REFERENCES

1. B. Stout, J.-C. Auger, and J. Lafait, "A transfer matrix approach to local field calculations in multiple scattering problems," J. Mod. Opt. **49**, 2129–2152 (2002).
2. J.-C. Auger and B. Stout, "A recursive centered T-matrix algorithm to solve the multiple scattering equation: numerical validation," J. Quant. Spectrosc. Radiat. Transf. **79–80**, 533–547 (2003).
3. A. Doicu and T. Wriedt, *Light Scattering by Systems of Particles* (Springer, 2006).
4. L. Tsang, J. A. Kong, and R. T. Shin, *Theory of Microwave Remote Sensing* (Wiley, 1985).
5. W. C. Chew, *Waves and Fields in Inhomogeneous Media* (IEEE Press, 1994).
6. M. Lax, "Multiple scattering of waves," Rev. Mod. Phys. **23**, 287–310 (1951).
7. B. Stout, C. Andraud, S. Stout, and J. Lafait, "Absorption in multiple scattering systems of coated spheres," J. Opt. Soc. Am. A **20**, 1050–1059 (2003).
8. B. Stout, J.-C. Auger, and J. Lafait, "Individual and aggregate scattering matrices and cross sections: conservation laws and reciprocity," J. Mod. Opt. **48**, 2105–2128 (2001).
9. D. W. Mackowski, "Calculation of total cross sections in multiple-sphere clusters," J. Opt. Soc. Am. A **11**, 2851–2861 (1994).
10. O. Moine and B. Stout, "Optical force calculations in arbitrary beams by use of the vector addition theorem," J. Opt. Soc. Am. B **22**, 1620–1631 (2005).
11. M. I. Mishchenko, L. D. Travis, and A. Lacis, *Scattering, Absorption and Emission of Light by Small Particles* (Cambridge U. Press, 2002).
12. C. F. Bohren and D. R. Huffman, *Absorption and Scattering of Light by Small Particles* (Wiley-Interscience, 1983).
13. D. E. Gray, ed., *American Institute of Physics Handbook*, 3rd ed. (McGraw-Hill, 1972).
14. Z. Li, M. Käll, and H. Xu, "Optical forces on interacting plasmonic nanoparticles in a focused Gaussian beam," Phys. Rev. B **77**, 085412 (2008).
15. S. Bidault, F. J. G. Abajo, and A. Polman, "Plasmon-based nanolenses assembled on a well-defined DNA template," J. Am. Chem. Soc. **130**, 2750–2751 (2008).